How to cite: *Angew. Chem. Int. Ed.* **2023**, *62*, e202303394
doi.org/10.1002/anie.202303394

Expanded Porphyrins

Bispalladium(II) Complexes of di-*p*-Pyrirubyrin Derivatives as Promising Near-Infrared Photoacoustic Dyes

Karolina Hurej, Weronika Oszczęda, Ewelina Opas, Szymon J. Zelewski, Miłosz Pawlicki, Michał J. Białek, Łukasz Orzeł, and Lechosław Latos-Grażyński*

Abstract: The insertion of palladium(II) into di-*p*-pyrirubyrin results in mutually convertible bimetallic complexes. Post-synthetic functionalization of one of them yielded bispalladium(II) dioxo-di-*p*-pyrirubyrin and, after demetallation, dioxo-di-*p*-pyrirubyrin, introducing for the first time the α,β′-pyridin-2-one unit into the macrocyclic frame. Bispalladium(II) di-*p*-pyrirubyrin **6**, bispalladium(II) dioxo-di-*p*-pyrirubyrin **9**, and dioxo-di-*p*-pyrirubyrin **10** absorb and emit light around 1000 nm and are characterized by high photostability. Thus, they are promising candidates for near-infrared photoacoustic dyes, ideally targeting (**9**) the wavelength of Yb-based fiber lasers. The incorporation of an α,β′-pyridine moiety into expanded porphyrins opens a highly interesting area of research due to the attractive optical and coordination properties of the resulting molecules.

Optical properties imprinted into strongly conjugated systems play a crucial role in contemporary research focusing on fundamentals of the interaction of organic or inorganic derivatives with visible light but also on the potential applicability of π-extended systems.[1] The expanded porphyrins, macrocyclic systems with typically improved conjugation and an increased delocalization pathway, have been extensively explored for their optical, electrochemical, and coordination properties.[2,3] In addition, due to a larger macrocyclic cavity, they have generated complexes containing more than one metal ion, efficiently increasing the conjugation.[4–6]

The metal complexes of rubyrins are still an underexplored group of compounds, with few examples based on metal coordination via pyrrole nitrogen atoms.[4a,7] Among them, there are coordination compounds of [26]rubyrin ([26]hexaphyrin(1.1.0.1.1.0)) with rhodium(I) (**1**), zinc(II), or iridium(III) ions.[8] Insertion of two Co^{II} cations into [26]rubyrin accompanied by two-electron ligand oxidation afforded the bis-Co^{II} complex of antiaromatic [24]rubyrin **2** (Scheme 1).[8] [26]Dioxohexaphyrin(1.1.1.1.1.1) provides a remarkable [NNNO] coordination core, as illustrated by paramagnetic bis-Cu^{II} compound **3** (Scheme 1) or diamagnetic bis-Ni^{II} complexes.[9] Incorporation of a pyridine unit into the expanded porphyrin core can be expected to result in specific coordination behaviour.[10–13] Thus, C,G-di-pyri-octaphyrin(1.1.0.0.1.1.0.0) revealed noteworthy coordination flexibility upon treatment with Pd^{II} ions as it converted to the C_i- (**4**) and C_s-symmetric [NNNC]-coordinated bis-Pd^{II} complexes.[10]

Considering their electronic properties, expanded porphyrins may be useful for biomedical imaging methods such as photoacoustic imaging (PAI).[14] PAI allows increasing the imaging depth and higher spatial resolution compared with traditional optical imaging, because biological tissues are more transparent to the acoustic output signal than they are to optical outputs.[15–17] Thus, copper(II) dioxohexaphyr-

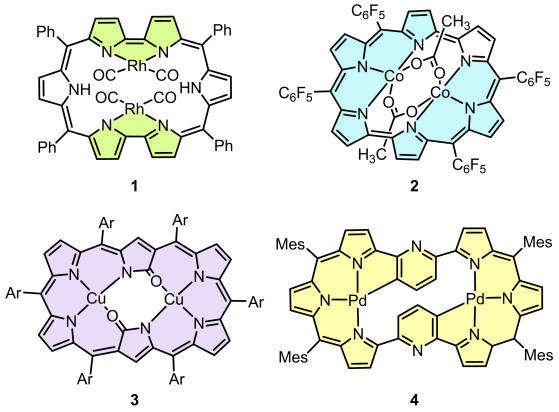

Scheme 1. Selected examples of expanded porphyrin complexes.

[*] Dr. K. Hurej, W. Oszczęda, E. Opas, Dr. M. J. Białek, Prof. L. Latos-Grażyński
Department of Chemistry, University of Wroclaw
F. Joliot-Curie 14, 50383 Wrocław (Poland)
E-mail: karolina.hurej@uwr.edu.pl
Dr. S. J. Zelewski
Department of Semiconductor Materials Engineering, Faculty of Fundamental Problems of Technology, Wrocław University of Science and Technology
Wyb. Wyspiańskiego 27, 50370 Wrocław (Poland)
and
Department of Physics, Cavendish Laboratory, University of Cambridge
JJ Thomson Avenue, Cambridge CB3 0HE (UK)
Prof. M. Pawlicki, Dr. Ł. Orzeł
Department of Chemistry, Jagiellonian University
Gronostajowa 2, 30358 Kraków (Poland)

in (**3**) gives a spectral response in the NIR-II range, a targeted area for deeper tissues imaging, providing higher maximum permissible exposure and reduced light scattering in biological material.[18] Significantly, octaphyrin derivatives encapsulated within organic nanoparticles can help visualize and discriminate between cancerous and healthy tissues.[19] Generally, the set of compounds that can be successfully applied in the second near-infrared window (1000–1700 nm) of photoacoustic imaging is rather limited.[20–22] Therefore, searching for compounds with an absorption wavelength above 1000 nm and high photostability is of great importance to further improve the depth of imaging.[23,24] Most photoacoustic dyes, such as regular porphyrin derivatives and their complexes, give a photoacoustic response, but usually to a higher energy range (700–1000 nm).[14,25–28]

We have previously reported the synthesis and reactivity of a new ligand, A,D-di-*p*-pyrirubyrin **5** (Scheme 2).[29] Herein, we present the synthesis and mutual transformations of bispalladium(II) di-*p*-pyrirubyrin complexes, including their regioselective oxygenation. The resulting incorporation of α,β′-pyridine-2-one, an unprecedented moiety in expanded porphyrin chemistry, into the rubyrin frame is of particular significance. The photoacoustic response of rubyrin derivatives, including in the NIR-II range, has also been explored.

The reaction of palladium(II) chloride with A,D-di-*p*-pyrirubyrin **5** in the presence of triethylamine (TEA) resulted in the insertion of two palladium(II) cations into the macrocyclic coordination core, producing **6** (Scheme 2). The symmetric complex **6** possesses two palladium(II) ions, each coordinating three nitrogen atoms and one chloride ion. In the mass spectrum of **6**, the apparent molecular peak $[M–Cl]^+$ was found at *m*/*z* 1183.2575. This value and the characteristic isotopic pattern prove the simultaneous coordination of two palladium(II) cations.

The X-ray-determined molecular structure of **6**[30] confirms that the palladium(II) cations acquire a nearly square-planar geometry and fit well within the 3 N subpockets. The Pd^{II} coordination spheres are supplemented with chloride anions pointing above and below the mean plane of the macrocycle (Figure 1). The Pd···Pd distance equals 4.4447 (12) Å.

The molecule possesses an inversion center; thus, the PdN3 units can be treated as a pair of enantiomers affording an achiral meso diastereomer.

The ^{1}H NMR spectrum of **6** collected in the lower temperature range (223–253 K) presents a pattern consistent with the C_i symmetry already encountered in the solid state.

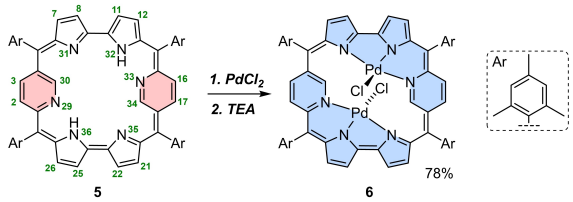

Scheme 2. Palladium(II) ions insertion into **5**.

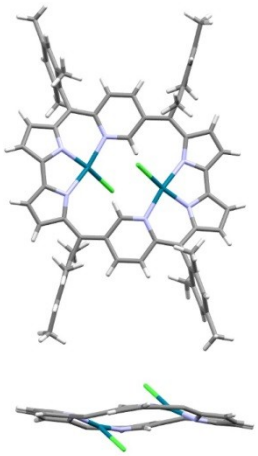

Figure 1. X-ray structure of **6**. In the side view, mesityl groups and selected H atoms are omitted for clarity.

The pyridine protons present an ABX pattern (CH(2,16) 10.32, CH(3,17) 10.17, C(30,34)H −2.41 ppm; Figure 2a). Still, the inversion with respect to the macrocyclic plane of **6** is reflected by the appropriate changes in the ^{1}H NMR spectra collected at 263–300 K (see Supporting Information).

The stepwise transformation of **6** into **7** and **8** (Scheme 3, top) has been detected by UV/Vis (Figure S3) and ^{1}H NMR (Figure 2) spectra.

The conversion of **6** into **7** can be described as a formal addition of HCl to **6**. It involves the heterolytic dissociation of the Pd–N(31) bond accompanied by the coordination of chloride and protonation of released N(31). The next step (**7** to **8**) is analogous, involving Pd–N(35) bond. Addition of a

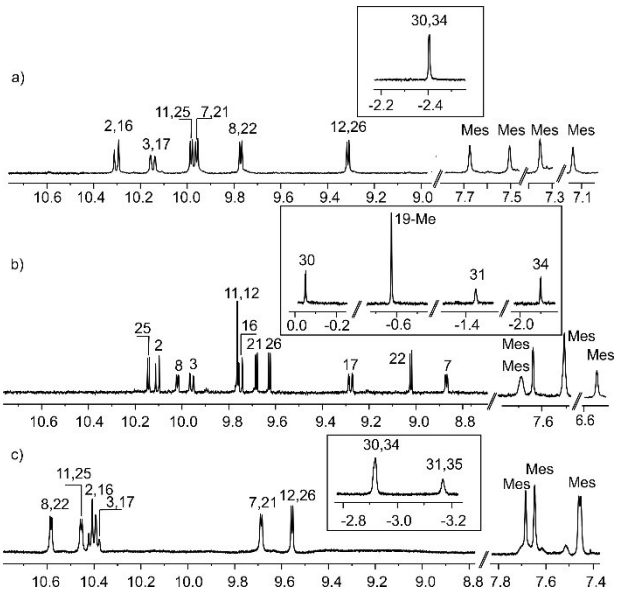

Figure 2. ^{1}H NMR spectra (selected regions) of a) **6**, b) **7** and c) **8** (500 MHz, chloroform-*d*; a) 238 K, b) and c) 300 K).

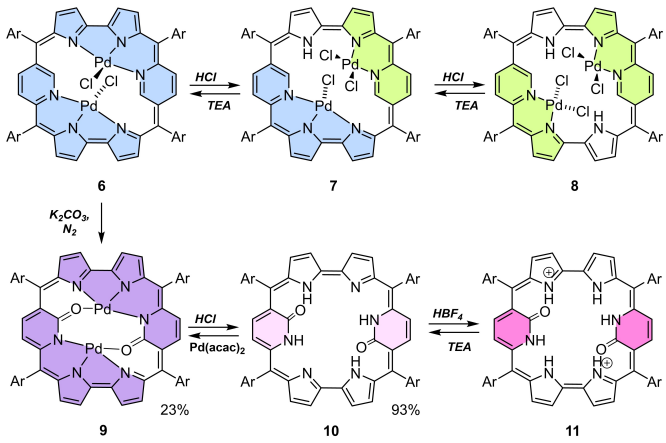

Scheme 3. Mutual transformations of **6**–**11**.

nitrogen base to solutions of **7** or **8** results in a quantitative recovery of **6**.

Upon the addition of acid, the Q bands at 970 and 810 nm shifted hypsochromically to 950 and 750 nm, respectively (see Figure S3).

The number of resonances in the ^{1}H NMR spectrum of **7** reflects its intrinsic asymmetry (Figure 2b). The characteristic signals from the outer and inner protons of two different pyridine rings have been identified as two ABX patterns (1. CH(2) 10.11, CH(3) 9.98, CH(30) −0.02 ppm; 2. CH(16) 9.76, CH(17) 9.28, CH(34) −2.10 ppm). Moreover, the methyl signal from the 19-*meso*-mesityl-substituent is shifted to a specific lower frequency region, down to −0.6 ppm, due to the interaction with the corrugated framework of **7** (Figure 3a). The broadened NH(31) resonance, reflecting HCl addition, has been spotted at −1.41 ppm.

The ^{1}H NMR features of **8** are clearly consistent with its C_i-symmetry (Figure 2c), which is visible already at 300 K. In addition, the ^{1}H NMR spectrum includes a typical ABX pattern of α,β′-pyridine moiety (CH(2,16) 10.39, CH(3,17), 10.36, CH(30) −2.91 ppm).

Structures **7** and **8** were subjected to DFT optimizations (Figure 3). Evidently, the palladium(II) coordination mode enforces the specific adjustment of the macrocyclic frame, as clearly reflected by the positions of atoms C(5), C(14), C(19), and C(28) in **5**, **6**, **7** and **8**. The nearly rectangular arrangement of **5'**s framework (C(5)···C(19) 9.539 Å, C-(14)···C(28) 9.904 Å) transforms to the parallelogrammical one (C(5)···C(19) 8.676 Å, C(14)···C(28) 10.390 Å) in **6**.

Finally, addition of HCl affords **8** (C(5)···C(19) 9.688 Å, C(14)···C(28) 9.876 Å), which acquires slightly deformed rectangular geometry again.

Due to the high potential of post-synthetic functionalization,[31] a specific transformation of **6** has been elaborated. Thus, a solution of **6** underwent a reaction with potassium carbonate to form bispalladium(II) dioxo-di-*p*-pyrirubyrin **9** (Scheme 3, bottom). The oxygenation occurs at two α′-positions of α,β′-pyridine units [C(30) and C(34)]. Palladium(II) coordination to three nitrogen donors is preserved. However, it is accompanied by the formation of a bond between palladium(II) and the incorporated oxygen atom, which replaced the chloride ligand in the parent compound **6**. Here, one can notice that dioxo-di-*p*-pyrirubyrin belongs to a novel class of porphyrinoids based on the incorporation of an unprecedented α,β′-pyridin-2-one moiety into a macrocyclic skeleton. Previously, only the α,α′-pyridin-3-one unit has been incorporated into the porphyrinic structure.[31]

The detailed mechanism of dioxygenation remains to be explored. Still, the appropriate analogy can be drawn based on the coordination chemistry and reactivity of metallopyridinates.[32] The nitrogen coordination of α,β′-pyridine to a palladium(II) center of **6** causes the regioselective activation of its α′-position towards nucleophilic reagents. An attack by hydroxide on **6** is expected to result in the formation of the transient covalent hydrate. Such a species can be invoked in further transformations (including oxidation) to form pyridin-2-one units incorporated into **9** or **10**.

Demetallation of **9** with hydrochloric acid vapors (from above the 37 %-water solution) followed by neutralization yields dioxo-di-*p*-pyrirubyrin **10**. The reaction of **10** with $Pd(acac)_2$ recovers **9** (Scheme 3, bottom).

The molecular structures of **9** and **10** were determined by X-ray crystallography[30] (Figure 4). All four donors [NNNO] for both palladium(II) cations are located in the macrocyclic plane of **9**. Pyridin-2-one is a bridging fragment linking two palladium(II) centers, applying its nitrogen and oxygen donors. The distortion of the donor-Pd-donor angles is up to 11° from the ideal 90°. The Pd···Pd distance is only minimally shorter than in **6** and equals 4.3985(11) Å. **10** adopts a planar geometry in the solid state, except for the slight tilt of the pyridin-2-one moieties. Instead of the metal ions, protonated nitrogen atoms from six-membered rings are present within inner lactam moieties. The bond patterns of α,β′-pyridin-2-one resemble the lactams such as for 4,5-dihydropyridin-2(3H)-one.[33] In both cases, the oxygen

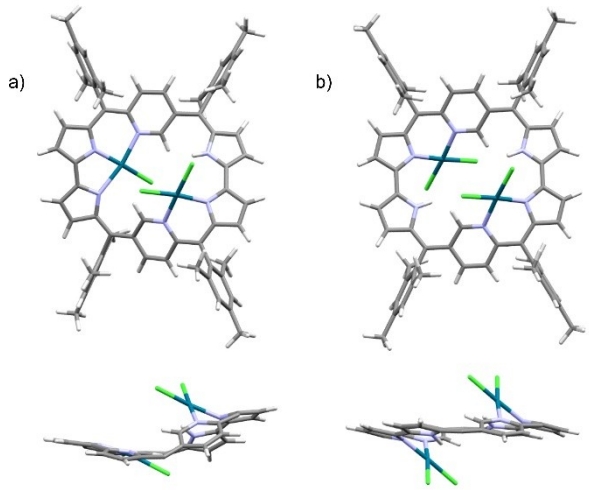

Figure 3. DFT-optimized molecular structures of **7** and **8**. In the side views, aryl groups are omitted for clarity.

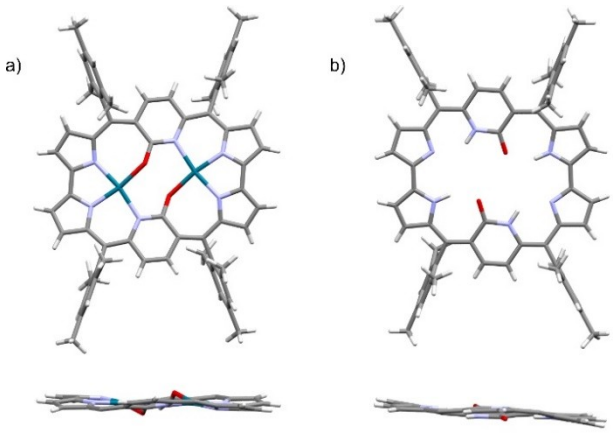

Figure 4. X-ray structures of a) **9**, b) **10**. In the side view, mesityl groups and selected H atoms are omitted for clarity.

atoms are slightly displaced from the mean macrocyclic plane ($\Delta C_{4meso} = 0.36$ Å for **10**, 0.49 Å for **9**).

The macrocycle detected in the solid state has C_i symmetry. However, the ^{1}H NMR spectrum of **9** (Figure 5a) reveals features corresponding to an effective C_{2h} symmetry. This implies fast conformational rearrangement. The process requires a concerted transfer of a carbonyl unit from one side of **9** to the other. The ^{1}H NMR spectrum of **10** resembles the pattern of its palladium(II) complex **9**. The pyridin-2-one protons attain an ABX pattern—CH(3,17) 11.38, CH(2,16) 10.57, NH(31,32) −0.68 ppm (Figure 5b).

This conversion from **10** to **11** with HBF_4 was followed by UV/Vis and NMR spectroscopy. After adding acid, the band recorded at 988 nm shifts hypsochromically by almost 40 nm to 950 nm (Figure S4). The ^{1}H NMR spectrum of **11** (Figure 5c) shows a similar pattern as that reported for **10**, reflecting the effective C_{2h} symmetry. However, in contrast to **5**,[29] for which the stepwise inversion of pyridine rings was detected for protonated forms, **11** preserves the structure of the neutral counterpart.

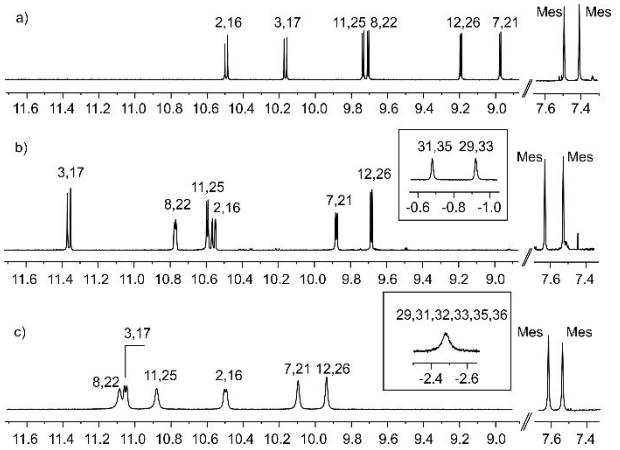

Figure 5. ^{1}H NMR spectra (selected regions) of a) **9**, b) **10** and c) **11** (500 MHz, chloroform-*d*, 300 K).

Electronic spectra were obtained for all discussed macrocyclic compounds (Figure 6). Each of them shows features characteristic of aromatic rubyrins and metallorubiryns[34] with the most red-shifted absorption band recorded at the border between NIR–I and NIR-II windows. The emission spectra showed that all four compounds (**5**, **6**, **9**, and **10**) exhibit photoluminescence with a small Stokes shift ($\Delta\lambda \approx 1$–12 nm, Figure 6), eventually reaching the NIR-II window of the wavelength covering the range of $\lambda_{EM} = 970$–1040 nm (Figure 6). The established quantum yields (QYs) for all four luminophores (**5** −0.023; **6** −0.012; **9** −0.024; **10** −0.068) show a different efficiency of the observed emission. Significantly, these compounds revealed the absorption and emission bands around the 950–1050 nm region meeting the fundamental requirement for chromophores to be used in the second near-infrared window of photoacoustic imaging.[20–22]

Photoacoustic spectra showed that **5**, **6**, **9**, and **10** demonstrate efficient photoacoustic responses upon excitation with NIR-II light, with intense sharp absorption bands in the NIR-II window (Figure 7). In the case of **5** and **10**, these responses were weaker than for their palladium(II) complexes **6** and **9**, matching the absorption spectra. Photoacoustic spectroscopy (PAS) is exclusively sensitive to the absorbed portion of the incident light, generating acoustic waves through material temperature elevation through non-radiative relaxation. Minute discrepancies between relative photoacoustic signal intensity compared to absorption spectra can be attributed to the neglected light scattering and different photoluminescence quantum yields between the compounds.

Furthermore, in photothermal deflection spectroscopy probing the material absorbance with a higher dynamic range than in photoacoustic spectroscopy, we observed a clear, relatively strong absorption edge in the NIR range for **5**, but not so much for other materials (Figure S54). The absorption onset, reaching a maximum of around 1 eV (≈1200 nm), is characterized by a distinct tail with an Urbach energy of ≈55 meV, comparable with alternative organic dye compounds such as conjugated polymers.[1,35]

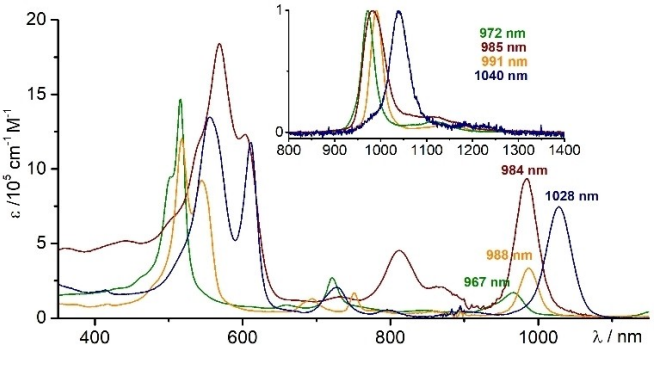

Figure 6. Absorption and emission spectra (inset) of **5** (green line, $\lambda_{ex} = 520$ nm), **6** (brown line, $\lambda_{ex} = 565$ nm), **9** (blue line, $\lambda_{ex} = 613$ nm), and **10** (yellow line, $\lambda_{ex} = 547$ nm). All spectra were recorded in CH_2Cl_2 solution.

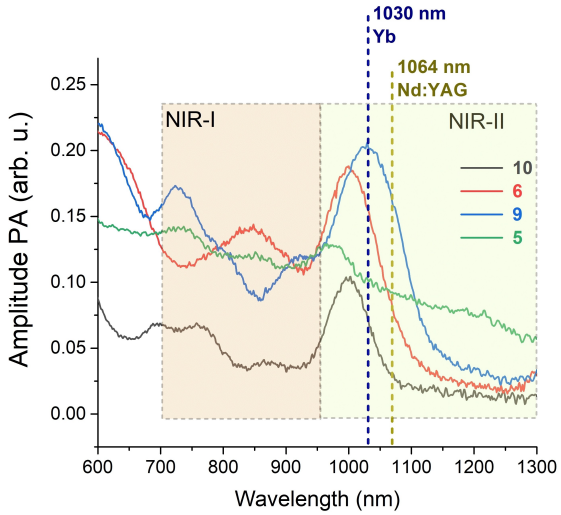

Figure 7. Photoacoustic spectra of **5**, **6**, **9**, and **10** (293 K, modulation frequency: 10 Hz, measurement taken on dried-down material, drop-casted from a chloroform solution onto microscope glass slides).

To test the photostability of the materials, we performed time-dependent measurements of the photoacoustic signal amplitude at the NIR-II absorption peak of each compound (Figure S56). Under the conditions used for spectroscopic characterization, the photoacoustic response remains unchanged, preserving the original intensity after 60 min of continuous excitation. That gives crucial evidence for the potential to perform reliable imaging experiments without photoinduced degradation of the dyes.

In conclusion, bispalladium(II) A,D-di-*p*-pyrirubyrin provided an effective scaffold for inner core dioxygenation to form bispalladium(II) dioxo-di-*p*-pyrirubyrin. A novel type of porphyrinoid based on the incorporation of the α,β′-pyridin-2-one unit into the macrocyclic skeleton has been described. Significantly, the investigated A,D-di-*p*-pyrirubyrin derivatives revealed absorptions and emissions around 1000 nm, high photostability, and efficient photoacoustic responses. Complex **9** ideally targets the wavelength of Yb-based fiber lasers (≈1030 nm), which made progress in industrial processing due to the excellent laser power/production cost ratio.[36,37] In the field of high-power pulsed NIR lasers, they proved to be affordable high-intensity sources for optically-excited imaging and other scientific applications, competing with popular Nd:YAG (neodymium-doped yttrium aluminum garnet) lasers and other solid-state solutions. Thus, it can be envisaged that the described properties of the modified rubyrins may be promising for their application as near-infrared photoacoustic dyes.

Acknowledgements

Financial support from the National Science Center (Grants 2019/35/D/ST4/00361, and for emission part: 2019/35/B/ST4/00318; M.P.) is kindly acknowledged. The Wrocław Supercomputer Centre (KDM WCSS) is kindly acknowledged for sharing computation resources necessary for DFT calculations (Grant 329). S.J.Z. acknowledges support from the Polish National Agency for Academic Exchange within the Bekker program (PPN/BEK/2020/1/00264/U/00001). The publication of this article was supported by the Excellence Initiative—Research University program for the University of Wrocław.

Conflict of Interest

The authors declare no conflict of interest.

Data Availability Statement

The data that support the findings of this study are available from the corresponding author upon reasonable request.

Keywords: Expanded Porphyrins · Near-Infrared II · Palladium · Photoacoustic Dyes · Rubyrin

[1] A. V. Fenukhin, A. G. Kazanskii, A. G. Kolosko, E. I. Terukov, A. V. Ziminov, *J. Non-Cryst. Solids* **2006**, *352*, 1668–1670.
[2] a) T. Tanaka, A. Osuka, *Chem. Rev.* **2017**, *117*, 2584–2640; b) V. V. Roznyatovskiy, C.-H. Lee, J. L. Sessler, *Chem. Soc. Rev.* **2013**, *42*, 1921–1933.
[3] Z. Zhang, D. S. Kim, C.-Y. Lin, H. Zhang, A. D. Lammer, V. M. Lynch, I. Popov, O. Š. Miljanić, E. V. Anslyn, J. L. Sessler, *J. Am. Chem. Soc.* **2015**, *137*, 7769–7774.
[4] a) B. Szyszko, M. J. Białek, E. Pacholska-Dudziak, L. Latos-Grażyński, *Chem. Rev.* **2017**, *117*, 2839–2909; b) B. Szyszko, L. Latos-Grażyński, *Angew. Chem. Int. Ed.* **2020**, *59*, 16874–16901.
[5] J. L. Sessler, E. Tomat, *Acc. Chem. Res.* **2007**, *40*, 371–379.
[6] W. Stawski, M. Kijewska, M. Pawlicki, *Chem. Asian J.* **2020**, *15*, 8–20.
[7] S. J. Narayanan, B. Sridevi, T. K. Chandrashekar, U. Englich, K. Ruhlandt-Senge, *Inorg. Chem.* **2001**, *40*, 1637–1645.
[8] T. Soya, A. Osuka, *Chem. Eur. J.* **2015**, *21*, 10639–10644.
[9] A. Srinivasan, T. Ishizuka, A. Osuka, H. Furuta, *J. Am. Chem. Soc.* **2003**, *125*, 878–879.
[10] L. Liu, Z. Hu, F. Zhang, Y. Liu, L. Xu, M. Zhou, T. Tanaka, A. Osuka, J. Song, *Nat. Commun.* **2020**, *11*, 6206.
[11] N. Rawat, A. Sinha, M. Ravikanth, *Chem. Asian J.* **2022**, *17*, e202101141.
[12] M. Das, B. Adinarayana, A. Srinivasan, *ACS Omega* **2021**, *6*, 35204–35212.
[13] M. Das, S. Chitranshi, M. Murugavel, B. Adinarayana, C. H. Suresh, A. Srinivasan, *Chem. Commun.* **2020**, *56*, 3551–3554.
[14] C. Li, C. Liu, Y. Fan, X. Ma, Y. Zhan, X. Lu, Y. Sun, *RSC Chem. Biol.* **2021**, *2*, 743–758.
[15] M. Xu, L. V. Wang, *Rev. Sci. Instrum.* **2006**, *77*, 041101.
[16] C. Yin, X. Li, Y. Wang, Y. Liang, S. Zhou, P. Zhao, C.-S. Lee, Q. Fan, W. Huang, *Adv. Funct. Mater.* **2021**, *31*, 2104650.
[17] K. Li, B. Liu, *Chem. Soc. Rev.* **2014**, *43*, 6570–6597.
[18] K. Shimomura, H. Kai, Y. Nakamura, Y. Hong, S. Mori, K. Miki, K. Ohe, Y. Notsuka, Y. Yamaoka, M. Ishida, D. Kim, H. Furuta, *J. Am. Chem. Soc.* **2020**, *142*, 4429–4437.
[19] J. Chen, A. C. Sedgwick, S. Sen, Y. Ren, Q. Sun, C. Chau, J. F. Arambula, T. Sarma, L. Song, J. L. Sessler, C. Liu, *Chem. Sci.* **2021**, *12*, 9916–9921.

[20] Y. W. Zhou, D. Wang, Y. Zhang, U. Chitgupi, J. Geng, Y. Wang, Y. Zhang, T. R. Cook, J. Xia, J. F. Lovell, *Theranostics* **2016**, *6*, 688–697.
[21] B. L. Park, K. M. Lee, S. Park, M. Yun, H. J. Choi, J. Kim, Ch. Lee, H. Kim, C. Kim, *Theranostics* **2020**, *10*, 2509–2521.
[22] C. Ou, Y. Zhang, W. Ge, L. Zhong, Y. Huang, W. Si, W. Wang, Y. Zhao, X. Dong, *Chem. Commun.* **2020**, *56*, 6281–6284.
[23] K. Huang, Y. Zhang, J. Lin, P. Huang, *Biomater. Sci.* **2019**, *7*, 472–479.
[24] X. Ge, Q. Fu, L. Bai, B. Chen, R. Wang, S. Gao, J. Song, *New J. Chem.* **2019**, *43*, 8835–8851.
[25] N. Toriumi, N. Asano, T. Ikeno, A. Muranaka, K. Hanaoka, Y. Urano, M. Uchiyama, *Angew. Chem. Int. Ed.* **2019**, *58*, 7788–7791.
[26] I. T. Ho, J. L. Sessler, S. S. Gambhir, J. V. Jokerst, *Analyst* **2015**, *140*, 3731–3737.
[27] I. T. Ho, Z. Zhang, M. Ishida, V. M. Lynch, W.-Y. Cha, Y. M. Sung, D. Kim, J. L. Sessler, *J. Am. Chem. Soc.* **2014**, *136*, 4281–4286.
[28] F. Wu, H. Su, Y. Cai, W.-K. Wong, W. Jiang, X. Zhu, *ACS Appl. Bio Mater.* **2018**, *1*, 110–117.
[29] R. Myśliborski, K. Hurej, M. Pawlicki, L. Latos-Grażyński, *Angew. Chem. Int. Ed.* **2018**, *57*, 16866–16870.
[30] Deposition Numbers 2252972 (for **6**) 2252974 (for **9**), 2252973 (for **10**) contain the supplementary crystallographic data for this paper. These data are provided free of charge by the joint Cambridge Crystallographic Data Centre and Fachinformationszentrum Karlsruhe Access Structures service.
[31] C. Brückner, *Acc. Chem. Res.* **2016**, *49*, 1080–1092.
[32] E. C. Constable, *Polyhedron* **2016**, *103*, 295–306.
[33] M. Hugener, H. Heimgartner, *Helv. Chim. Acta* **1995**, *78*, 1863–1878.
[34] S. J. Narayanan, B. Sridevi, T. K. Chandrashekar, A. Vij, R. Roy, *J. Am. Chem. Soc.* **1999**, *121*, 9053–9068.
[35] X. Shi, X. Liao, K. Gao, L. Zuo, J. Chen, J. Zhao, F. Liu, Y. Chen, A. K.-Y. Jen, *Adv. Funct. Mater.* **2018**, *28*, 1802324.
[36] T.-Y. Tsai, Z.-C. Lee, *Opt. Lett.* **2020**, *45*, 17–20.
[37] B. Sun, J. Jia, J. Huang, X. Zhang, J. Bai, *Laser Phys.* **2017**, *27*, 105105.

Manuscript received: March 7, 2023
Accepted manuscript online: May 13, 2023
Version of record online: June 2, 2023